Supporting Information

Selective Electrochemical CO_2 Conversions to Multicarbon Alcohols on Highly Efficient N-doped Porous Carbon-supported Cu Catalysts

Hyunsu Han[a], *Yuseong Noh*[a], *Yoongon Kim*[a], *Seongmin Park*[a], *Wongeun Yoon*[a], *Daehee Jang*[a], *Sung Mook Choi*[b] and *Won Bae Kim*[a]*

[a] Department of Chemical Engineering, Pohang University of Science and Technology (POSTECH), 77 Cheongam-ro, Nam-gu, Pohang, Gyeongbuk, 37673, Republic of Korea

[b] Materials Center for Energy Department, Surface Technology Division, Korea Institute of Materials Science, Changwon, 642831, Republic of Korea

---

*Corresponding author
Tel: 82-54-279-2397
Fax: 82-54-279-5528
E-Mail: kimwb@postech.ac.kr

Table S1. Textural properties of various carbon materials.

Samples	BET surface area (m^2 g^{-1})	Total pore volume (cm^3 g^{-1})	Micropore volume (cm^3 g^{-1})	Meso-Macro pore volume (cm^3 g^{-1})
PC	684	0.59	0.36	0.23
NPC-700	661	0.61	0.37	0.24
NPC-800	651	0.58	0.38	0.20
NPC-900	634	0.55	0.33	0.22

Table S2. Chemical compositions and CO_2 uptake of various carbon materials.

Samples	N (at. %)	Graphitic N (%)	Pyridinic N (%)	Oxidized N (%)	Pyrrolic N (%)	CO_2 uptake (mmol g^{-1})
PC	-	-	-	-	-	0.45
NPC-700	11.2	35.5	26.7	10.5	27.3	1.62
NPC-800	10.9	38.8	37.5	9.6	14.1	2.26
NPC-900	9.6	46.9	24.9	20.9	7.3	1.20

Table S3. Contents of total N with various N species of Cu/NPC hybrid catalysts.

Samples	N (at. %)[a]	Graphitic N (%)	Pyridinic N (%)	Oxidized N (%)	Pyrrolic N (%)
Cu/NPC-700	8.5	29.1	30.5	11.6	28.8
Cu/NPC-800	8.4	32.7	40.8	10.6	15.9
Cu/NPC-900	7.1	40.3	27.9	22.1	9.7

[a] determined by XPS analysis.

Table S4. Cu particle sizes, Cu contents and analytical results of the Cu $2p_{3/2}$ spectra of Cu/PC and Cu/NPC hybrid catalysts.

Samples	Cu (wt. %)[a]	Average particle size (nm)[b]	Binding energy (eV)[c]
			$Cu^0 + Cu^+$
Cu/PC	21.6	12.1	932.2
Cu/NPC-700	19.7	5.3	932.6
Cu/NPC-800	19.8	5.2	932.7
Cu/NPC-900	20.2	5.4	932.6

[a] determined by ICP spectrometer.

[b] determined by TEM.

[c] detemmined by XPS analysis.

Table S5. Chemical compositions of Cu/NPC hybrid catalysts obtained by the linear combination of XANES spectra.

Samples	Cu^0	Cu^+	Cu^{2+}
Cu/PC	0.871	0.073	0.056
Cu/NPC-700	0.721	0.147	0.132
Cu/NPC-800	0.716	0.159	0.125
Cu/NPC-900	0.727	0.142	0.131

Table S6. Average Faradaic efficiencies (%) of products obtained from electrocatalytic CO_2 reduction on PC and NPC materials at different potentials.

PC								
E (V vs RHE)	CO	HCOOH	C_2H_4	C_2H_5OH	C_3H_7OH	H_2	Etc. (CH_3CHO,CH_3CH_2CHO)	Total
– 0.6	N.D.[a]	N.D.	N.D.	N.D.	N.D.	98.4	N.D.	98.4
– 0.7	N.D.	N.D.	N.D.	N.D.	N.D.	97	N.D.	97
– 0.8	N.D.	N.D.	N.D.	N.D.	N.D.	98.2	N.D.	98.2
– 0.9	N.D.	1.1	N.D.	N.D.	N.D.	96.3	N.D.	97.4
– 1.0	N.D.	2	N.D.	N.D.	N.D.	95.1	N.D.	97.1
– 1.05	N.D.	0.8	N.D.	N.D.	N.D.	97	N.D.	97.8
– 1.1	N.D.	N.D.	N.D.	N.D.	N.D.	98.2	N.D.	98.2
NPC-700								
E (V vs RHE)	CO	HCOOH	C_2H_4	C_2H_5OH	C_3H_7OH	H_2	Etc. (CH_3CHO,CH_3CH_2CHO)	Total
– 0.6	34.8	N.D.	N.D.	N.D.	N.D.	61.9	N.D.	96.7
– 0.7	40.3	3.2	N.D.	N.D.	N.D.	53.8	N.D.	97.3
– 0.8	42.6	4.7	N.D.	N.D.	N.D.	50.9	N.D.	98.2
– 0.9	48.8	5.7	N.D.	N.D.	N.D.	43.2	N.D.	97.7
– 1.0	50.8	6	N.D.	N.D.	N.D.	40.8	N.D.	97.6
– 1.05	50.5	4.1	N.D.	N.D.	N.D.	44.3	N.D.	98.9
– 1.1	49.7	2.7	N.D.	N.D.	N.D.	45.8	N.D.	98.2
NPC-800								
E (V vs RHE)	CO	HCOOH	C_2H_4	C_2H_5OH	C_3H_7OH	H_2	Etc. (CH_3CHO,CH_3CH_2CHO)	Total
– 0.6	48.7	N.D.	N.D.	N.D.	N.D.	49.5	N.D.	98.2
– 0.7	50.0	1.5	N.D.	N.D.	N.D.	45.6	N.D.	97.1
– 0.8	56.6	2.7	N.D.	N.D.	N.D.	38.1	N.D.	97.4
– 0.9	59.1	3.7	N.D.	N.D.	N.D.	36.2	N.D.	99
– 1.0	61.8	4.6	N.D.	N.D.	N.D.	30.7	N.D.	97.1
– 1.05	61.3	3.4	N.D.	N.D.	N.D.	32.7	N.D.	97.4
– 1.1	60.1	1.6	N.D.	N.D.	N.D.	36.4	N.D.	98.1
NPC-900								
E (V vs RHE)	CO	HCOOH	C_2H_4	C_2H_5OH	C_3H_7OH	H_2	Etc. (CH_3CHO,CH_3CH_2CHO)	Total
– 0.6	30.5	N.D.	N.D.	N.D.	N.D.	68.2	N.D.	98.7
– 0.7	31.7	5.5	N.D.	N.D.	N.D.	59.5	N.D.	96.7
– 0.8	33.2	5.8	N.D.	N.D.	N.D.	57.8	N.D.	96.8
– 0.9	37.8	7.7	N.D.	N.D.	N.D.	51.6	N.D.	97.1
– 1.0	41.6	8.9	N.D.	N.D.	N.D.	47.8	N.D.	98.3
– 1.05	41.9	6.2	N.D.	N.D.	N.D.	50.6	N.D.	98.7
– 1.1	39.7	3.1	N.D.	N.D.	N.D.	54.8	N.D.	97.6

[a] N.D. – Not detected. This is also applicable to Table S6-S7 and Table S10.

Table S7. Average Faradaic efficiencies (%) of products obtained from electrocatalytic CO_2 reduction on Cu/PC and Cu/NPC hybrid catalysts at different potentials.

E (V vs RHE)	CO	HCOOH	C_2H_4	C_2H_5OH	C_3H_7OH	H_2	Etc. (CH_3CHO, CH_3CH_2CHO)	Total
Cu/PC								
– 0.6	7.4	10.1	12.3	3.1	N.D.	65.0	N.D.	97.9
– 0.7	5.1	8.5	19.7	5.6	N.D.	58.7	N.D.	97.6
– 0.8	4.1	6.3	22.1	12.8	0.5	52.5	0.5	98.8
– 0.9	3.2	5.4	24.5	17.3	0.9	49.1	0.3	100.7
– 1.0	1.8	3.1	28.2	13.5	2.1	49.6	N.D.	98.3
– 1.05	1.1	1.8	30.7	10.5	1.1	52.6	0.2	98.0
– 1.1	0.5	0.3	30.4	9.7	0.4	56.4	N.D.	97.7
Cu/NPC-700								
– 0.6	20.5	N.D.	N.D.	29.6	0.5	46.6	1.5	98.7
– 0.7	17.4	N.D.	2	33.1	0.8	45.1	1.4	99.8
– 0.8	16.5	N.D.	2.6	40.1	1.3	38.9	1.1	100.5
– 0.9	12.3	N.D.	2.9	43.5	2.4	37.1	0.7	98.9
– 1.0	11.5	N.D.	3.4	45.2	4.2	33.1	0.8	98.2
– 1.05	4.3	N.D.	5.1	50.3	6.1	33.6	0.3	99.7
– 1.1	3.7	N.D.	6.8	45.5	4.1	38.3	0.4	98.8
Cu/NPC-800								
– 0.6	29.5	N.D.	N.D.	37.6	0.9	30	1.8	99.8
– 0.7	26.7	N.D.	N.D.	46	1.3	23.8	1.7	99.5
– 0.8	21.0	N.D.	1.8	51.4	2.0	22.2	1.4	99.8
– 0.9	17.9	N.D.	2.1	55.3	4.3	17.6	1.3	98.5
– 1.0	15.4	N.D.	2.9	58.8	6.2	13.2	0.8	97.3
– 1.05	7.1	N.D.	3.6	64.6	8.7	14.8	0.6	99.4
– 1.1	6.9	N.D.	4.4	60.1	5.5	19.7	0.6	97.2
Cu/NPC-900								
– 0.6	15.5	N.D.	N.D.	26.8	0.3	54.6	1.2	98.4
– 0.7	12.6	N.D.	3.2	29.7	0.5	51.8	1.1	98.9
– 0.8	10.5	N.D.	3.8	35.8	0.9	47.5	0.8	99.3
– 0.9	8.4	N.D.	4.7	38.9	1.4	44.6	0.6	98.6
– 1.0	6.5	N.D.	6.6	40.5	2.7	41.1	0.6	97.4
– 1.05	2.1	N.D.	7.3	44.4	4.3	42.1	0.1	100.3
– 1.1	1.5	N.D.	9.2	39.5	2.3	45.6	0.2	98.3

Table S8. Comparison of multicarbon product formation from various Cu-based catalysts.

Catalyst	Electrolyte	V (vs RHE)/ j_{total} (mA cm^{-2})	C2-C3 product (Faradaic efficiency, %)	Ref.
Cu/NPC-800	0.2 M $KHCO_3$	−1.05/12.6	C_2H_4 (3.6%), C_2H_5OH (64.6%), C_3H_7OH (8.7%)	This work
Cu foil	0.1 M $KHCO_3$	−1.05/5.8	C2-C3 products (40.6%) C_2H_4 (26%), C_2H_5OH (9.8%), C_3H_7OH (2.5%)	S1
Cu_2O derived Cu with $PdCl_2$	0.1 M $KHCO_3$	−1.0/19.5	C_2H_6 (30.1%), C_2H_5OH (11.1%), C_3H_7OH (5.5%)	S2
Cl-induced Cu_2O-Cu	0.1 M KCl	−1.8/7.7	C2-C4 products (55.1%) C_2H_4 (23%), C_2H_5OH (20%), C_3H_7OH (7.8%), C_3H_8 (1%), C_4H_{10} (1%)	S3
Nanostructured polycrystalline Cu (KF cycled)	0.1 M $KHCO_3$	−1.0/6.5	C2-C3 products (28%) C_2H_4 (16.3%), C_2H_5OH (7.85%), C_3H_7OH (3.08%)	S4
Cu oxide film (1.7 μm)	0.1 M $KHCO_3$	−0.99/30	C_2H_4 (38.79%), C_2H_5OH (9.01%)	S5
Oxide-reduced agglomerated Cu nanoparticles	0.1 M $KHCO_3$	−0.95/19.9	C_2H_4 (35.82%), C_2H_5OH (12.75%), C_3H_7OH (8.75%)	S6
Cu_2O derived Cu films (sample C)	0.1 M $KHCO_3$	−0.98/26.2	C_2H_4 (31%), C_2H_5OH (7.1%), C_3H_7OH (3.7%)	S7
Cu/N-doped graphene	0.1 M $KHCO_3$	−1.2/1.2	C_2H_5OH (63%)	S8
Single crystals Cu (100)	0.1 M $KHCO_3$	−1/5	C2-C3 products (57.8%) C_2H_4 (40.4%), C_2H_5OH (9.7%), C_3H_7OH (1.5%)	S9
Cu (711)/ [4(100)·(111)]	0.1 M $KHCO_3$	−0.94/5	C2-C3 products (71.5%) C_2H_4 (50%), C_2H_5OH (7.4%), C_3H_7OH (4.6%)	
CuAu nanowire arrays	0.1 M $KHCO_3$	−0.7/1[a]	C_2H_5OH (~ 45%)	14
AuCu alloy embedded Cu submicrocone	0.5 M $KHCO_3$	−1/5.6 ± 0.77[a]	C_2H_4 (16±4%), C_2H_5OH (29±4%)	15
Hydrophobic Cu dendrite	0.1 M KPi	−1.3/30	C_2H_4 (7.56%), C_2H_6 (0.05%), C_2H_5OH (3.15%), CH_3COOH (1.37%)	16
Wettable Cu dendrite	0.1 M KPi	−0.94/30	C_2H_4 (3.61%), C_2H_6 (0.5%), C_2H_5OH (2.21%), CH_3COOH (0.34%), C_3H_7OH (1.37%)	

[a] Partial current density of C_2H_5OH.

Reference for Table S8.

[S1] K. P. Kuhl, E. R. Cave, D. N. Abram and T. F. Jaramillo, *Energy Environ. Sci*. 2012, **5**, 7050.

[S2] C. S. Chen, J. H. Wan and B. S. Yeo, *J. Phys. Chem*. C 2015, **119**, 26875–26882.

[S3] S. Lee, D. Kim and J. Lee, *Angew. Chem. Int. Ed*. 2015, **54**, 14701–14705.

[S4] Y. Kwon, Y. Lum, E. L. Clark, J. W. Ager and A. T. Bell, *ChemElectroChem* 2016, **3**, 1012–1019.

[S5] D. Ren, Y. Deng, A. D. Handoko, C. S. Chen, S. Malkhandi and B. S. Yeo, *ACS Catal*. 2015, **5**, 2814–2821.

[S6] D. Ren, N. T. Wong, A. D. Handoko, Y. Huang and B. S. Yeo, *J. Phys. Chem. Lett*. 2016, **7**, 20–24.

[S7] A. D. Handoko, C. W. Ong, Y. Huang, Z. G. Lee, L. Lin, G. B. Panetti and B. S. Yeo, *J. Phys. Chem. C* 2016, **120**, 20058–20067.

[S8] Y. Song, R. Peng, D. K. Hensley, P. V. Bonnesen, L. Liang, Z. Wu, H. M. Meyer, M. Chi, C. Ma, B. G. Sumpter and A. J. Rondinone, *ChemistrySelect* 2016, **1**, 6055–6061.

[S9] Y. Hori, I. Takahashi, O. Koga and N. Hoshi, *J. Mol. Catal. Chem*. 2003, **199**, 39–47.

Table S9. Physicochemical characterizations of Cu10/NPC-800 and Cu30/NPC-800.

Samples	Cu loading (wt. %)[a]	Particle size (nm)[b]	N content (at. %)[c]	Pyridinic N (%)	Binding energy (eV)[c]
					$Cu^0 + Cu^+$
Cu10/NPC-800	9.4	5.0	9.1	37.6	932.5
Cu30/NPC-800	31.7	6.3	5.8	39.3	932.7

[a] determined by ICP spectrometer.
[b] determined by TEM.
[c] determined by XPS analysis.

Table S10. Average Faradaic efficiencies (%) of products obtained from electrocatalytic CO_2 reduction on Cu10/NPC-800 and Cu30/NPC-800 at different potentials.

Cu10/NPC-800								
E (V vs RHE)	CO	HCOOH	C_2H_4	C_2H_5OH	C_3H_7OH	H_2	Etc. (CH_3CHO, CH_3CH_2CHO)	Total
– 0.6	39.5	N.D.	N.D.	6.5	0.1	51.6	N.D.	97.6
– 0.7	42.7	1.2	N.D.	8.0	0.2	44.8	0.6	97.3
– 0.8	38.6	1.4	N.D.	13.4	0.4	42.1	0.5	96.4
– 0.9	35.9	2.7	1.0	20.3	0.9	36.2	0.5	97.5
– 1.0	33.2	2.5	1.2	25.5	1.3	33.7	0.4	97.8
– 1.05	26.5	1.2	1.7	31.4	2.3	35.4	0.2	98.7
– 1.1	24.3	1.0	2.0	26.6	1.6	42.7	0.2	98.4
Cu30/NPC-800								
E (V vs RHE)	CO	HCOOH	C_2H_4	C_2H_5OH	C_3H_7OH	H_2	Etc. (CH_3CHO, CH_3CH_2CHO)	Total
– 0.6	8.5	N.D.	8.2	18.8	0.2	62.0	0.7	98.2
– 0.7	6.7	N.D.	9.6	23.5	0.3	57.8	0.6	98.5
– 0.8	5.3	N.D.	12.1	24.1	0.7	55.2	0.4	97.7
– 0.9	4.5	N.D.	15.5	29.3	1.0	46.6	0.3	97.2
– 1.0	3.3	N.D.	18.8	32.8	1.9	41.2	0.3	98.3
– 1.05	0.8	N.D.	19.5	35.6	2.7	41.4	0.1	100.1
– 1.1	0.4	N.D.	21.9	31.1	1.8	43.7	0.2	99.1

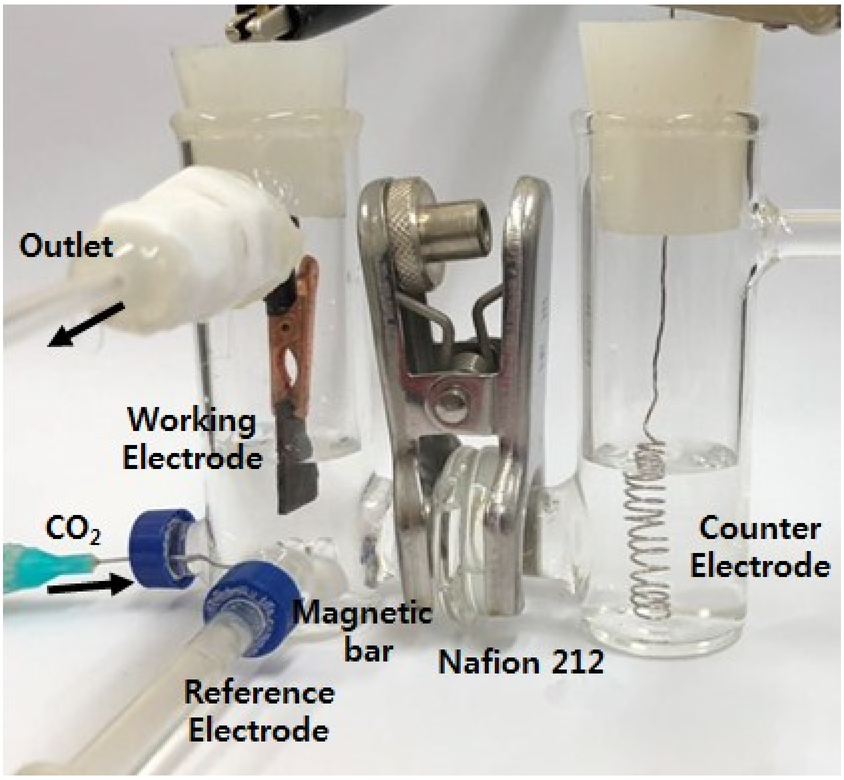

Fig. S1 Photograph of H-type cell for electrocatalytic CO_2 reduction.

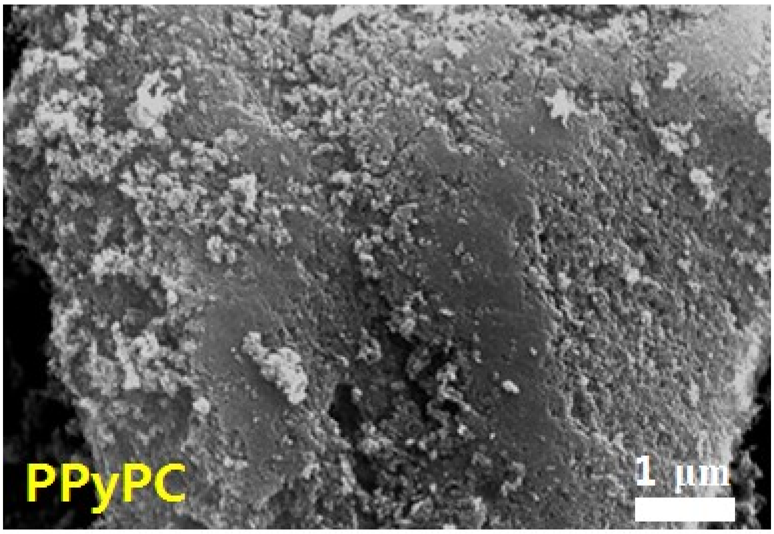

Fig. S2 SEM images of PPyPC.

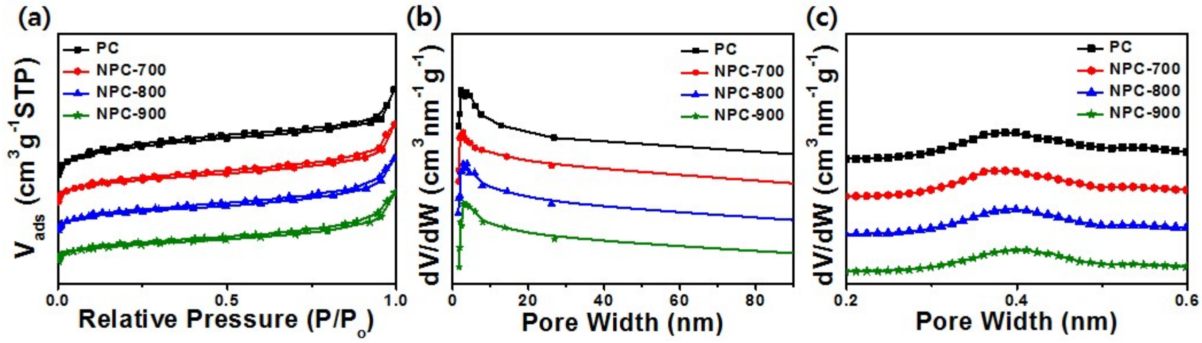

Fig. S3 (a) N_2 adsorption/desorption isotherms and pore size distributions calculated by (b) Barrett-Joyner-Halenda (BJH) and (c) Horváth-Kawazoe (HK) method for PC, NPC-700, NPC-800 and NPC-900.

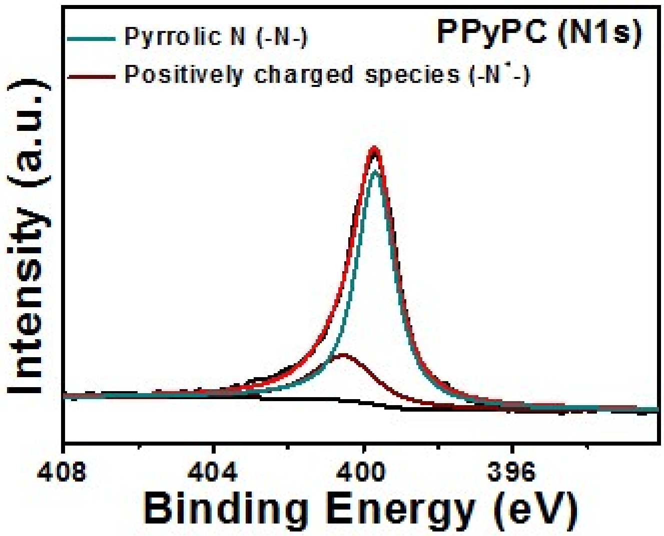

Fig. S4 High resolution N 1s spectra of PPyPC.

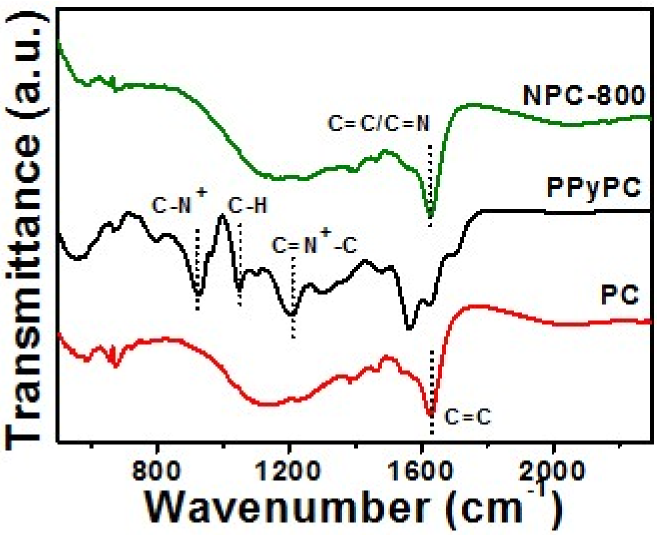

Fig. S5 FTIR spectroscopy of PC, PPyPC and NPC-800.

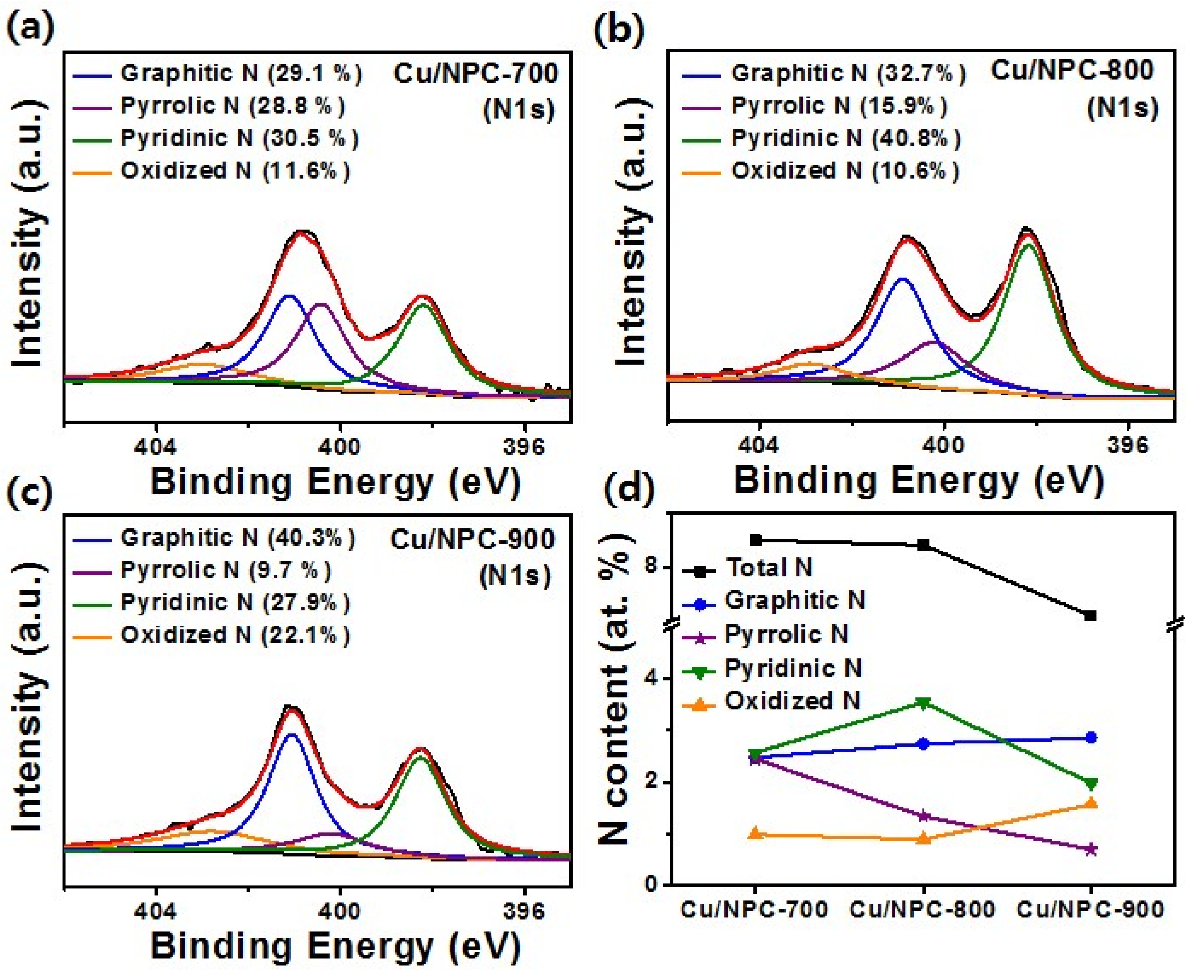

Fig. S6 High resolution N 1s spectra of (a) Cu/NPC-700, (b) Cu/NPC-800 and (c) Cu/NPC-900. (d) Summary of N atomic contents and relative concentrations.

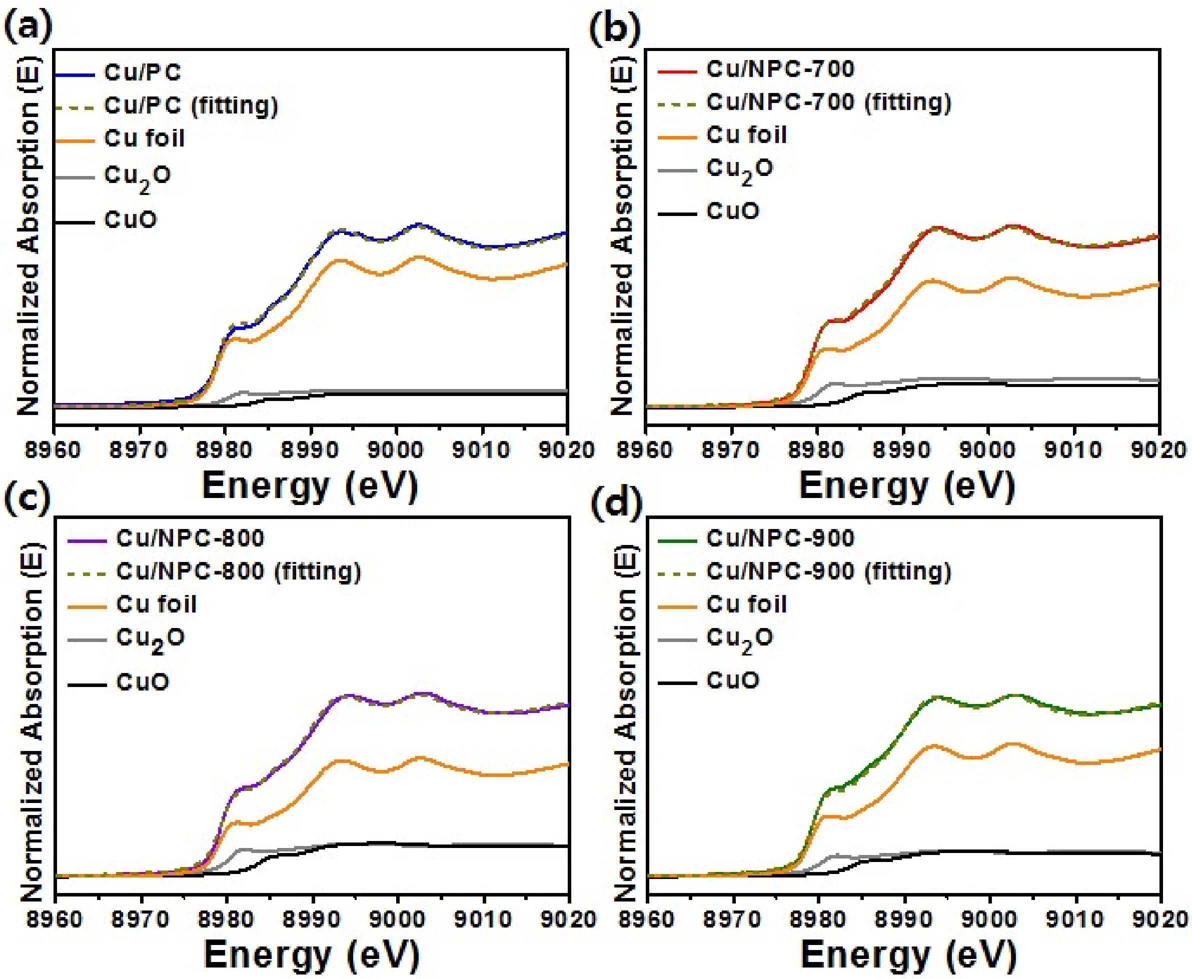

Fig. S7 Cu K-edge XANES fittings for Cu/PC, Cu/NPC-700, Cu/NPC-800 and Cu/NPC-900 by linear combination fittings (LCF). Dashed line is the fitted result.

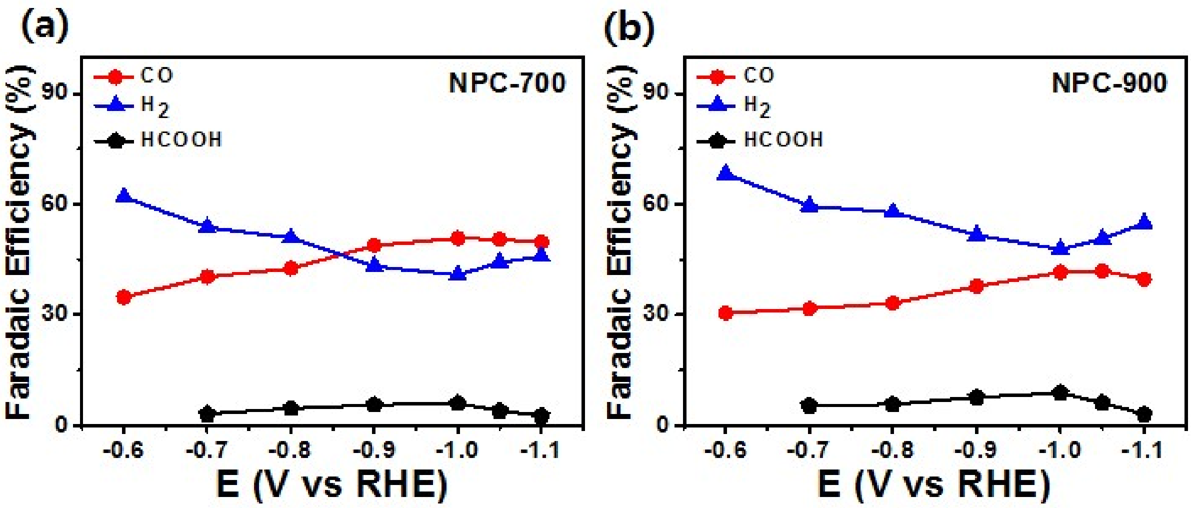

Fig. S8 Faradaic efficiencies of liquid and gaseous products for CO_2 reduction in CO_2-saturated 0.2 M $KHCO_3$ aqueous solution on (a) NPC-700 and (b) NPC-900.

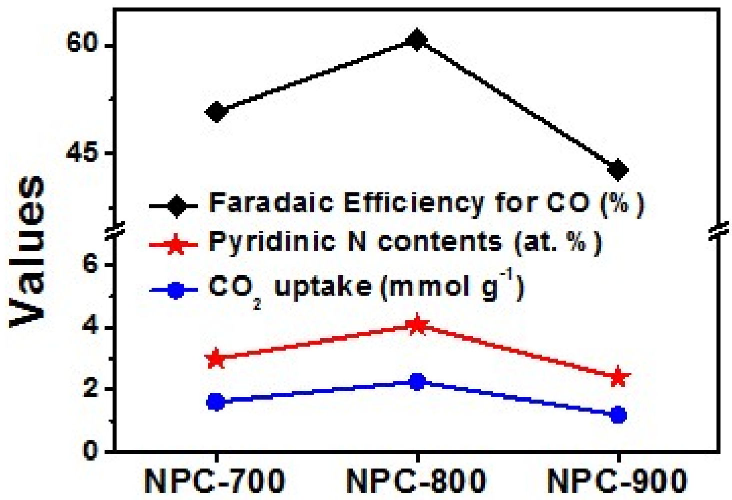

Fig. S9 Trend in maximum Faradaic efficiency for CO production versus contents of pyridinic N species and CO_2 uptake on NPC-700, NPC-800 and NPC-900.

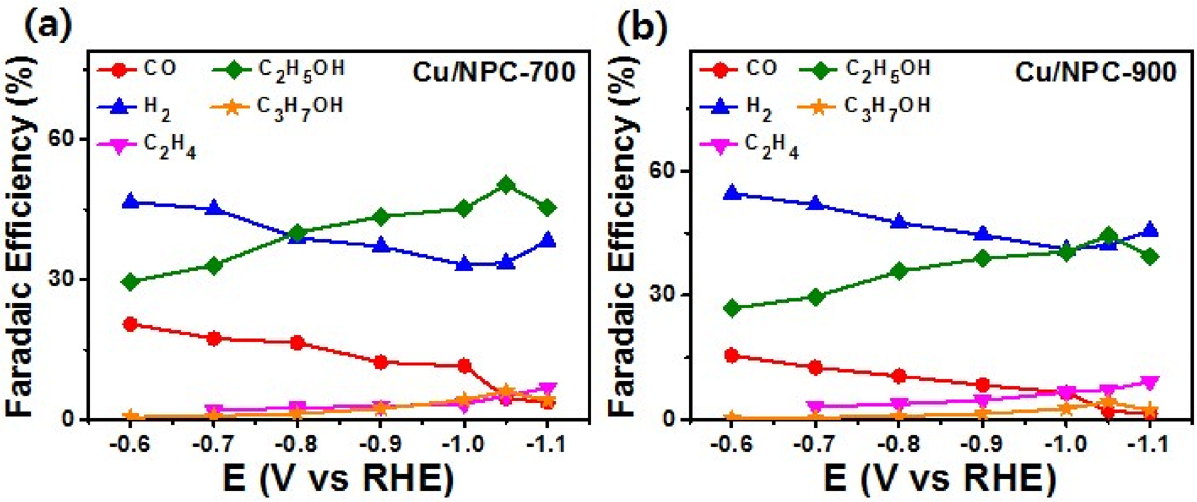

Fig. S10 Faradaic efficiencies of liquid and gaseous products for CO_2 reduction in CO_2-saturated 0.2 M $KHCO_3$ aqueous solution on (a) Cu/NPC-700 and (b) Cu/NPC-900.

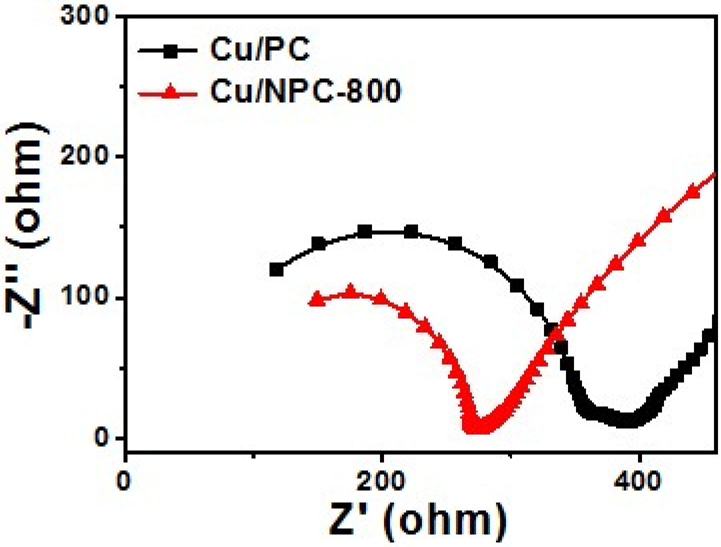

Fig. S11 EIS results of Cu/PC and Cu/NPC-800 performed in CO_2-saturated 0.2 M $KHCO_3$ aqueous solution at –1.05 V (vs RHE).

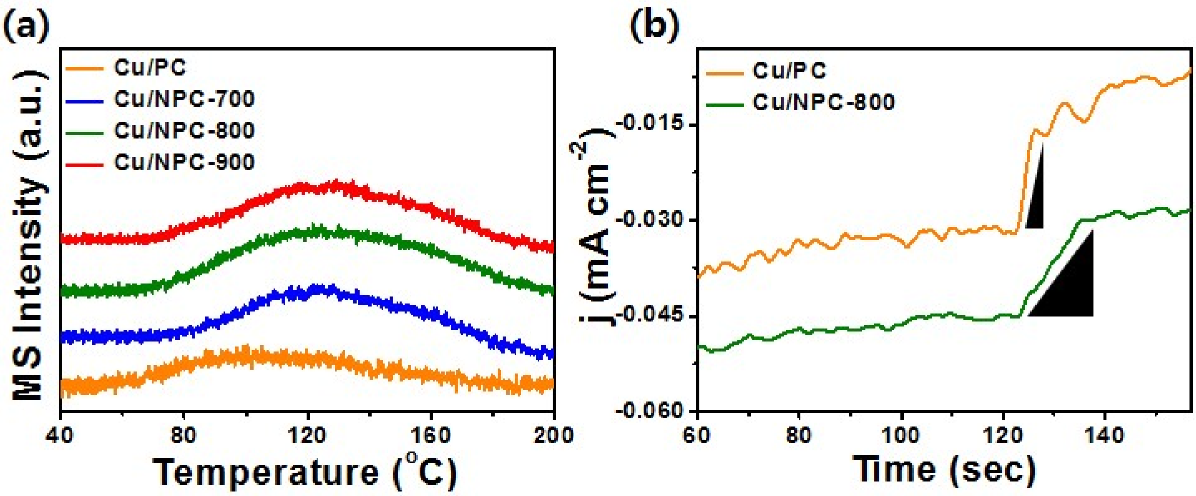

Fig. S12 Experimental measurements of CO adsorption strength on prepared catalysts. (a) CO-TPD profiles of Cu/PC, Cu/NPC-700, Cu/NPC-800 and Cu/NPC-900 at ramping rate of 5 °C min^{-1}. (b) Chronoamperometric measurements of Cu/PC and Cu/NPC-800 at constant potential of –0.12 V (vs RHE) in 0.2 M $KHCO_3$ aqueous solution.

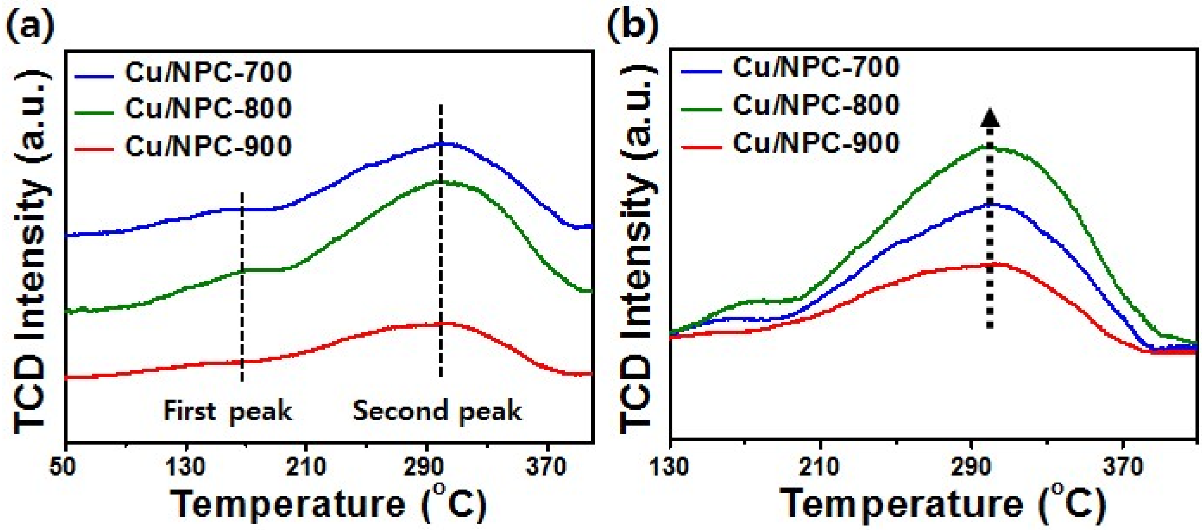

Fig. S13 (a) CO_2-TPD profiles of Cu/NPC-700, Cu/NPC-800 and Cu/NPC-900 measured at ramping rate of 10 °C min^{-1} and (b) the peak comparison of CO_2-TPD profiles.

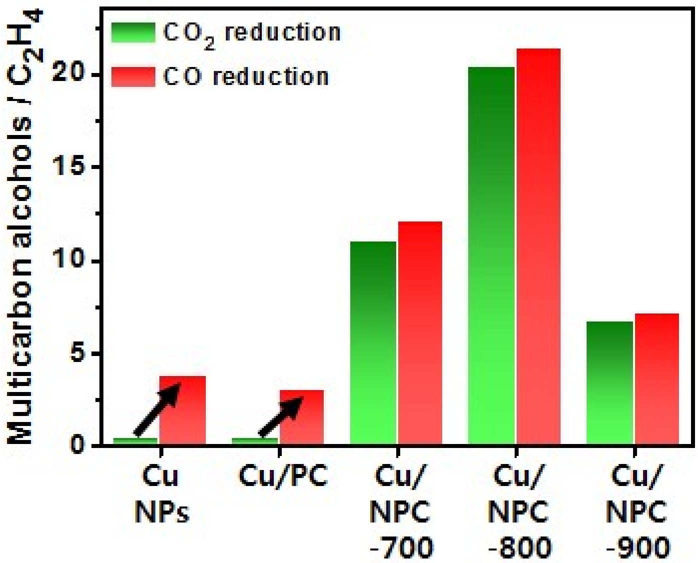

Fig. S14 Comparison of the relative ratio of Faradaic efficiencies of multicarbon alcohols to C_2H_4 for Cu catalysts in CO_2 reduction and CO reduction.

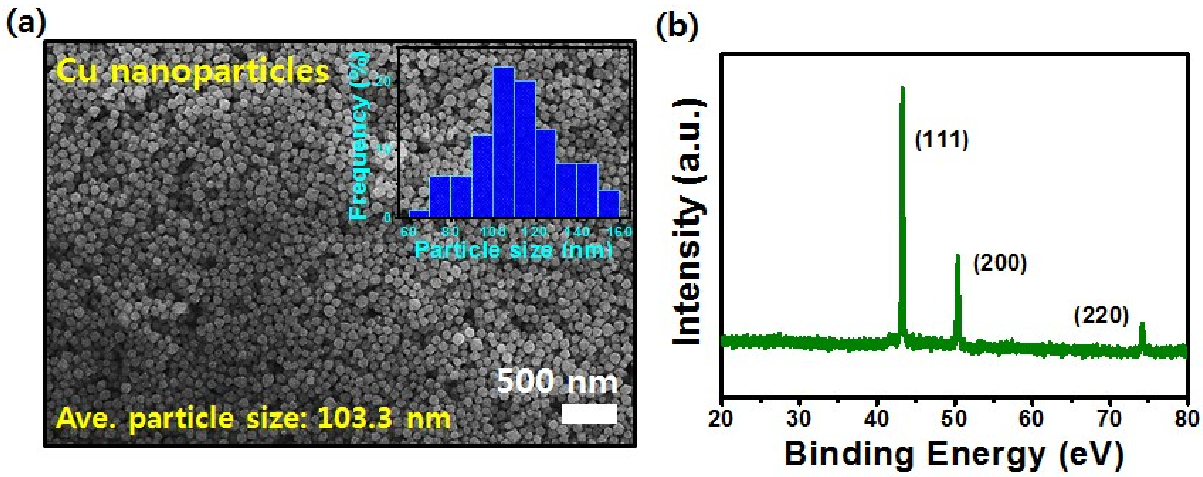

Fig. S15 (a) SEM image with particle size distribution of Cu nanoparticles and (b) the corresponding XRD patterns.

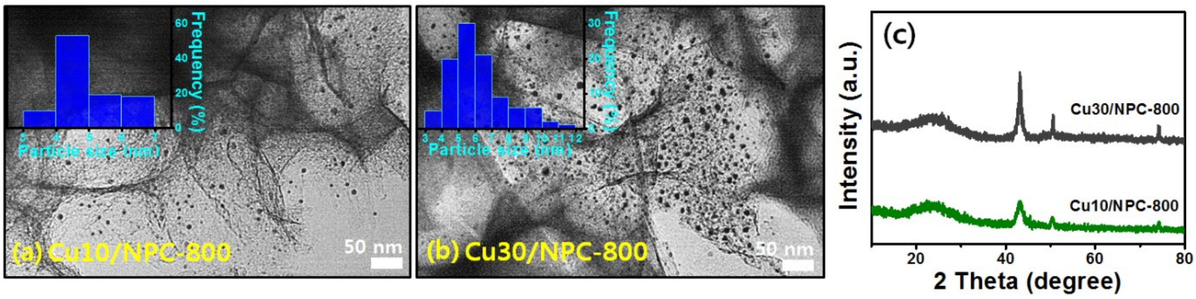

Fig. S16 TEM image with particle size distribution of (a) Cu10/NPC-800 and (b) Cu30/NPC-800 and (c) the corresponding XRD patterns.

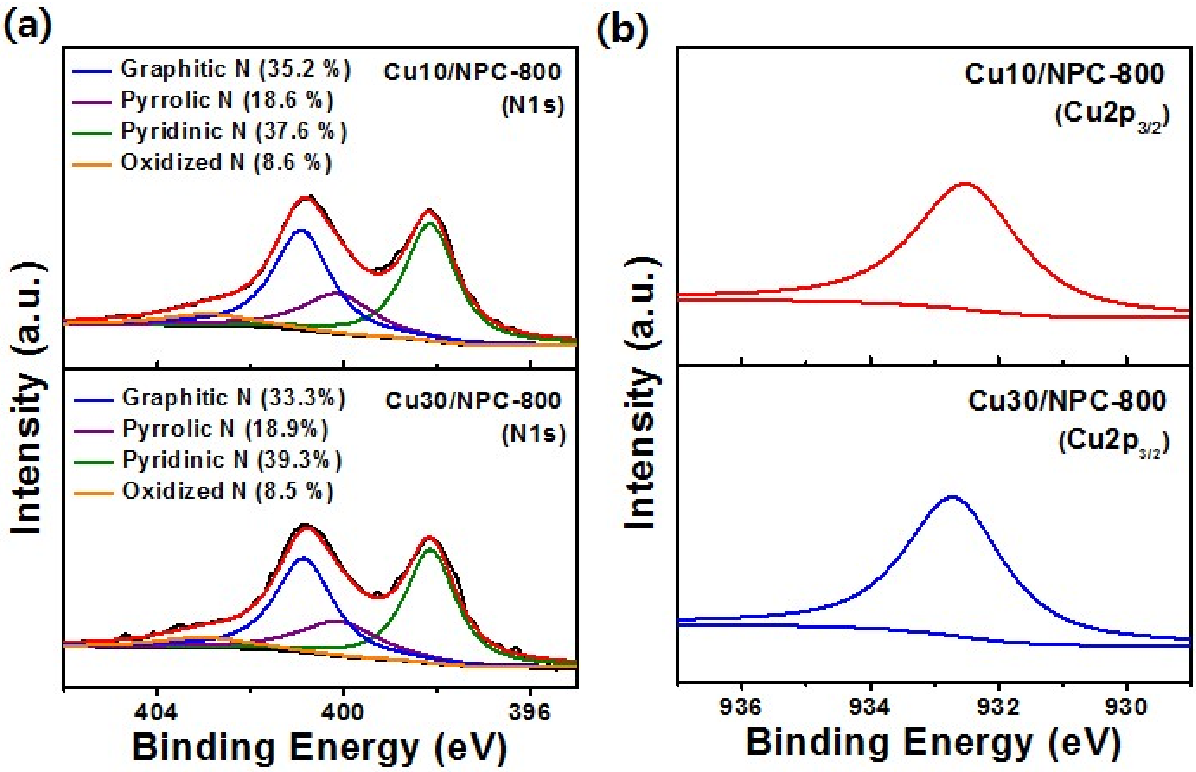

Fig. S17 (a) High resolution N 1s and (b) Cu $2p_{3/2}$ spectra of Cu10/NPC-800 and Cu30/NPC-800.

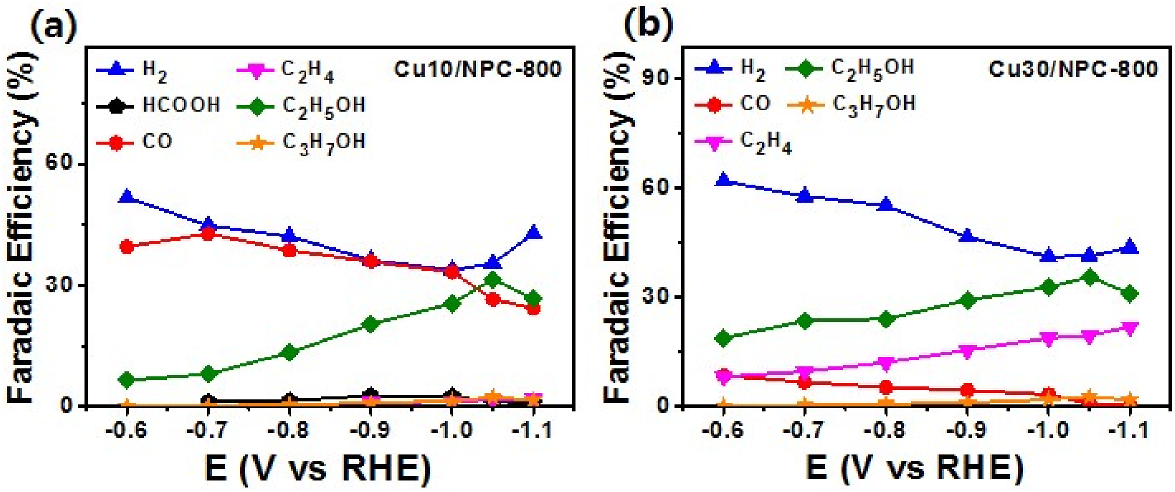

Fig. S18 Faradaic efficiencies of liquid and gaseous products for CO_2 reduction in CO_2-saturated 0.2 M $KHCO_3$ aqueous solution on (a) Cu10/NPC-800 and (b) Cu30/NPC-800.